Journal of Applied Mechanics and Technical Physics, Vol. 51, No. 4, pp. 471–481, 2010

FINITE-AMPLITUDE SOLITARY WAVES IN A TWO-LAYER FLUID

N. V. Gavrilov and V. Yu. Liapidevskii

UDC 532.59

Second-mode nonlinear internal waves at a thin interface between homogeneous layers of immiscible fluids of different densities have been studied theoretically and experimentally. A mathematical model is proposed to describe the generation, interaction, and decay of solitary internal waves which arise during intrusion of a fluid with intermediate density into the interlayer. An exact solution which specifies the shape of solitary waves symmetric about the unperturbed interface is constructed, and the limiting transition for finite-amplitude waves at the interlayer thickness vanishing is substantiated. The fine structure of the flow in the vicinity of a solitary wave and its effect on horizontal mass transfer during propagation of short intrusions have been studied experimentally. It is shown that, with friction at the interfaces taken into account, the mathematical model adequately describes the variation in the phase and amplitude characteristics of solitary waves during their propagation.

Key words: *solitary wave, two-layer fluid, shallow-water equations, intrusion, gravity flow.*

Introduction. Generation of internal waves in a density-stratified medium is an effective mechanism for transformation of large-scale flows in the ocean and atmosphere to smaller-scale motions with the subsequent dissipation of the energy of the wave. In the sea shelf area, nonlinear internal waves generated by tides or resulting from the interaction of flows with the bottom relief propagate toward the coast in the form of trains of solitary waves. A characteristic feature of both bottom and subsurface internal waves of large amplitude is their ability to transfer fluid and impurity particles for considerable distances. Recently, the structure of such flow has been actively studied both theoretically and experimentally. In stratified water reservoirs, internal waves with a trapped core have been found in the bottom layer [1] and the surface layer [2], and at the interface between homogeneous fluid layers of different densities [3]. Intrusion flows in the form of symmetric solitary waves at the interface between fluids have been studied using experimental and theoretical methods [4–11]. Interest in this class of flows is motivated by their unique ability to transfer mass along high-gradient interlayers in a stratified fluid due to the initial horizontal momentum. Solitary-wave flow is similar to vortex-ring flow [12], with the entrainment of the surrounding fluid and the vertical velocity component in rotational motion being effectively suppressed by stable stratification.

In the present work, symmetric solitary waves at the interface of a two-layer fluid were studied experimentally. Analytical and numerical solutions of the problem of propagation of large-amplitude internal waves in intrusion and gravity flows are constructed using a mathematical model of two-layer shallow water [13] which takes into account nonlinearity and dispersion.

1. Experimental Setup. The experiments were performed in a laboratory tank (Fig. 1) 140 cm long, 20 cm wide, and 35 cm deep, whose side walls and bottom were made of transparent Plexiglas [14]. The tank end of length $l_0 = 20$ cm was separated by a sealed partition which could be lifted and lowered to form a solitary wave.

Before the experiments, the partition was lifted and the tank was filled with layers of immiscible fluids of different densities ρ^+ and ρ^-. The layers had the same thickness H. The working fluids were fresh water and a weak solution of sugar in water. In all experiments, the relative difference in density between the layers $\varepsilon = (\rho^- - \rho^+)/\rho^+$ was not more than 0.005, which did not lead to a significant increase in the viscosity of the fluids. Sugar was used

Lavrent'ev Institute of Hydrodynamics, Siberian Division, Russian Academy of Sciences, Novosibirsk 630090. Novosibirsk State University, Novosibirsk 630090; gavrilov@hydro.nsc.ru; liapid@hydro.nsc.ru. Translated from Prikladnaya Mekhanika i Tekhnicheskaya Fizika, Vol. 51, No. 4, pp. 26–38, July–August, 2010. Original article submitted January 25, 2010.

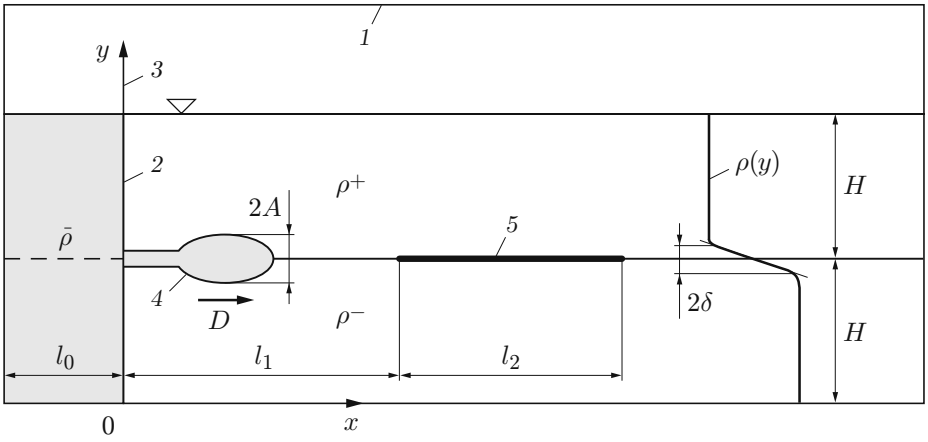

Fig. 1. Diagram of the experimental setup: 1) tank wall; 2) tank end; 3) sealed partition; 4) solitary wave; 5) thin plate.

to produce stratification since its diffusion coefficient is much lower than, for example, the diffusion coefficient of table salt. This made it possible to reduce the thickness of the diffusive zone. After the filling of the tank, a density distribution was established between the layers, which is well approximated by the formula

$$\rho(y) = \bar\rho + \frac{\rho^- - \rho^+}{2} \tanh\Big(\frac{y - H}{\delta}\Big), \tag{1.1}$$

where $\bar\rho = (\rho^- + \rho^+)/2$, 2δ is the characteristic thickness of the pycnocline, y is the vertical coordinate directed upward relative to the bottom of the tank, and ρ^+ and ρ^- are asymptotic values of the density in the upper and lower fluid layers, respectively.

A weak solution of sugar of the required density was produced by careful mixing of appropriate volumes of a high-density solution ($\varepsilon = 0.05$) and fresh water. The density of the concentrated solution was measured by a standard areometer with an error of 0.05%. The experiments were performed immediately after the filling of the tank; therefore, the thickness of the interlayer 2δ was approximately the same, and before the beginning of the experiments, it did not exceed $2\delta = 1.2$ cm, which was checked by an electrical conductivity sensor with a horizontal sensing element [15].

After the filling of the tank, the sealed partition was lowered. The fluid in section 2 (see Fig. 1) was carefully mixed and slightly colored, and according to formula (1.1), a mean density $\bar\rho$ was established in it. After removal of the partition, the fluid from the section flowed along the interface between the layers to the main part of the tank, and the fluid from the main part of the tank flowed along the bottom and the free surface to the end section. Then, the partition was lowered, resulting in the generation of a second-mode solitary wave 4 at the interface between the layers at some distance from the partition. Waves of different intensities were produced by varying the time during which the partition was open.

Solitary-wave propagation was recorded by a digital video camera (25 frames/sec) located at 2.5 m from the tank. As in experiments [16], the flow pattern was visualized as follows: a uniformly illuminated screen with inclined lines drawn on it (Fig. 2) was photographed through the fluid thickness. In the zones with a high density gradient, a characteristic deviation of these lines was observed, and in mixing zones, the optical transparency of the fluid was reduced. It should be noted that in the zones of increasing density gradient, the lines are seemingly denser, and in the zones of deceasing density gradient, they diverge. Above and below the pycnocline and in the solitary wave, the lines are not distorted, and, hence, the fluid in these regions is homogenous in density. The fluid of intermediate density propagating in the form of an intrusion along the interface is slightly colored with ink to visualize mass transfer (see Fig. 2).

In some experiments, a thin plate 5 was placed horizontally at the interface between the layers to study the transition from a short intrusion to gravity flow (see Fig. 1). (The distance from the partition 3 to the leading edge of the plate was $l_1 = 45$ cm, and plate length was $l_2 = 30$ cm.) Figure 2 gives photographs of the waves propagating immediately after the filling of the tank ($2\delta = 1.2$ cm) and after the passage of the first wave ($2\delta = 1.6$ cm). It

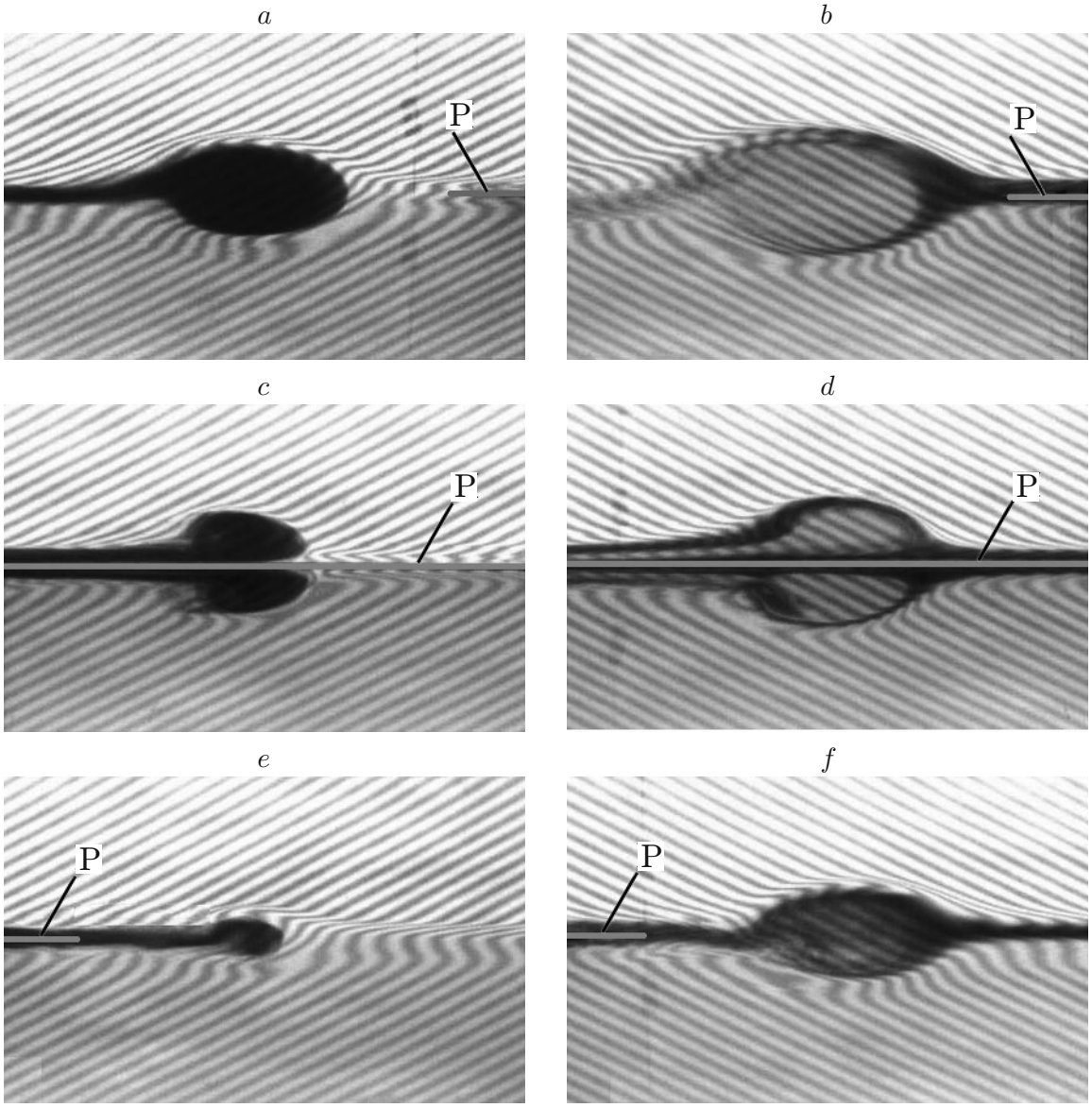

Fig. 2. Photographs of internal solitary waves incident on a horizontal plate (P) ($H = 8$ cm and $b = 2.5$ cm/sec^2): (a, c, e) wave propagation in the unperturbed layer ($\delta = 0.6$ cm); (b, d, f) after the passage of the first wave ($\delta = 0.8$ cm); (a, b) ahead of the plate; (c, d) on the plate; (e, f) behind the plate.

is evident from Fig. 2 that the incidence of the solitary wave onto the plate leads to a sudden change in the flow: the wave profile lost its symmetry, and a region of intense mixing is observed behind the wave head, i.e., the main features of gravity flow appear. These changes are most pronounced in the case of a thin initial interlayer (Fig. 2a, c, and e). Even a small increase in the interlayer thickness after the passage of the first wave is sufficient to prevent a significant distortion of the next wave in the vicinity of the plate (Fig. 2b, d, and f). The photographs presented in Fig. 2 also show the difference between the intrusion flows at the interface between the fluids and the gravity flows in the vicinity of the bottom or the lead of the channel due to the friction effect on the flow structure. Below, we construct exact solutions describing solitary waves within the framework of a dissipationless model and discuss the friction effect on the evolution of solitary waves at the interface between fluids and in the vicinity of the plate.

2. Mathematical Models of Two-Layer Shallow Water. As noted above, in the case of weak stratification $[(\rho^- - \rho^+)/\rho^+ \ll 1]$, flows symmetric about the central line of the channel can be implemented by intrusion of a fluid of intermediate density $\bar\rho = (\rho^- + \rho^+)/2$ into the layer between the homogeneous layers. In this case, it is sufficient to consider flows only in the lower part of the channel $(0 < y < H)$ and use a two-layer flow scheme to describe the evolution of the waves. In a long-wave approximation, nonlinear and dispersion effects are taken into account in model [17]. The two-layer model is determined by the dimensional quantities ρ^+, H, and $b = \varepsilon g/2$ (g acceleration of gravity). In the dimensionless variables $\rho^+ = 1$, $H = 1$, and $b = 1$, we assume that h and u are the depth and mean velocity of motion of the lower layer, ζ and w are the depth and velocity of the layer in the upper part of the flow region considered, and p is the pressure at the interface. We also assume that

$$\zeta = 1 - h, \qquad Q = hu + \zeta w = 0,$$
$$\frac{d_1}{dt} = \frac{\partial}{\partial t} + w\,\frac{\partial}{\partial x}, \qquad \frac{d_2}{dt} = \frac{\partial}{\partial t} + u\,\frac{\partial}{\partial x}. \tag{2.1}$$

In the Boussinesq approximation $[(\rho^- - \rho^+)/\rho^+ \ll 1]$, the model [17] is represented by the following system of equations [18]:

$$h_t + (hu)_x = 0,$$
$$u_t + uu_x + \frac{1}{3h}\left(h^2\,\frac{d_2^2 h}{dt^2}\right)_x + h_x + p_x = 0, \tag{2.2}$$
$$w_t + ww_x + \frac{1}{3\zeta}\left(\zeta^2\,\frac{d_1^2 \zeta}{dt^2}\right)_x + p_x = 0.$$

For flows in a two-layer fluid with a thin initial interlayer between homogeneous layers $\zeta_0 = 1 - h_0 \ll 1$, the mass conservation law in each layer implies that the velocity of particle motion in the intrusion is close to the wave velocity. Therefore, the vertical acceleration of particles in this region can be ignored, and in relations (2.2), the pressure in the upper layer can be replaced by hydrostatic pressure. Thus, system (2.1), (2.2) is simplified [13]:

$$h_t + (hu)_x = 0,$$
$$u_t + uu_x + \frac{1}{3h}\left(h^2\,\frac{d^2 h}{dt^2}\right)_x + h_x + p_x = 0, \tag{2.3}$$
$$w_t + ww_x + p_x = 0,$$
$$\frac{d}{dt} = \frac{\partial}{\partial t} + u\,\frac{\partial}{\partial x}.$$

Further simplification of Eqs. (2.3) is possible for $|u| \ll 1$ and $|h - h_0| \ll 1$. The corresponding weakly nonlinear model suitable for describing small-amplitude waves becomes [17]

$$h_t + (hu)_x = 0,$$
$$u_t + uu_x + h_0 h_{ttx}/3 + h_x + p_x = 0, \tag{2.4}$$
$$w_t + ww_x + p_x = 0.$$

Next, we analytically study solutions (2.2)–(2.4) which describe symmetric solitary waves at the interface between homogeneous layers of different densities.

For the three models presented above, we consider traveling waves, i.e., solutions of Eqs. (2.2)–(2.4) which depend on the variable $\xi = x - Dt$ ($D \equiv \text{const}$). We also require that for $|\xi| \to \infty$,

$$h \to h_0, \qquad h' \to 0, \qquad h'' \to 0 \tag{2.5}$$

(here and below, the prime denotes differentiation with respect to the variable ξ), i.e., the solutions are solitary waves.

We first consider traveling waves for the weakly nonlinear model (2.4). System (2.4) reduces to the following system of ordinary differential equations:

$$h(D-u)=h_0D, \qquad (1-h)(D-w)=(1-h_0)D,$$
$$(u-D)^2/2+h+h_0D^2h''/3-(w-D)^2/2=h_0. \tag{2.6}$$

In view of (2.5), Eq. (2.6) can be integrated and presented in the form of one ordinary differential equation for the function $h=h(\xi)$:

$$(h')^2=G_1(h)=\frac{3(h-h_0)^2(\mathrm{Fr}^2-h+h^2)}{\mathrm{Fr}^2\,h_0h(1-h)}. \tag{2.7}$$

Similarly, by virtue of (2.5) Eqs. (2.2) and (2.3) can be reduced to the differential equations

$$(h')^2=G_2(h)=\frac{3(h-h_0)^2(\mathrm{Fr}^2-h+h^2)}{\mathrm{Fr}^2\,h_0^2(1-h)}; \tag{2.8}$$

$$(h')^2=G_3(h)=\frac{3(h-h_0)^2(\mathrm{Fr}^2-h+h^2)}{\mathrm{Fr}^2(h_0^2(1-h)+(1-h_0)^2h)}, \tag{2.9}$$

where $\mathrm{Fr}=D/\sqrt{bH}=D$ is the Froude number.

We note that Eq. (2.7) follows immediately from (2.6), Eq. (2.8) was obtained in [13], and Eq. (2.9) is derived using the Boussinesq approximation from the corresponding representation for traveling waves in [17] (see, for example, formula (13) in [18]). We also note that the parameter

$$h_m=\left(1+\sqrt{1-4\,\mathrm{Fr}^2}\,\right)/2 \tag{2.10}$$

does not depend on the initial thickness of the upper layer $\zeta_0=1-h_0$; therefore, the functions G_i $(i=1,2,3)$ differ only in the denominator, and the common numerator vanishes for $h=h_0$ and $h=h_m$ $(0<h<1)$. As $h_0\to 1$, the functions G_i $(i=2,3)$ have the common limit

$$G_0(h)=3(1-h)(\mathrm{Fr}^2-h+h^2)/\,\mathrm{Fr}^2\,.$$

For models (2.2) and (2.3), the equation

$$(h')^2=G_0(h) \tag{2.11}$$

specifies the shape of the symmetric solitary wave propagating at the interface between the homogeneous layers ($\zeta_0=0$). For the models considered above, including the limiting case $h_0\to 1$, the wave profiles are found from relations (2.7)–(2.9) and (2.11) in quadratures

$$\xi=\xi_i(h)=\pm\int\limits_{h_m}^{h}\frac{ds}{\sqrt{G_i(s)}}, \qquad i=0,1,2,3. \tag{2.12}$$

We restrict the further consideration to the case $h_m<h_0$ which corresponds to the class of intrusion flows described in Sec. 1. Figure 3 shows curves of $y=G_i(h)$ $(i=0,1,2,3)$ for $h_0=0.95$ and $\mathrm{Fr}=0.40$ and 0.48. From Fig. 3 it follows that at a thin initial interlayer between homogeneous layers obtained experimentally, the graphs of the functions $y=G_2(h)$ and $y=G_3(h)$ almost coincide. Consequently, the corresponding models give close profiles of solitary symmetric waves propagating along the interface between fluids of different densities. Therefore, for numerical calculations of nonstationary intrusion flows in a channel, we shall use the simpler model (2.3).

We note that for traveling waves, Eq. (2.10) leads to the constraint $\mathrm{Fr}<\mathrm{Fr}_*=0.5$ and independence of the solitary-wave amplitude $A=2(1-h_m)$ on the initial thickness of the layer $\zeta_0=1-h_0$. This is equally valid for all models considered above. Since the root $h=h_0$ of the equation $G_i(h)=0$ is multiple for $h_0<1$, the dependence $h=h_i(\xi)$ obtained from (2.12) describes the soliton-like solution of the corresponding system of equations for $i=1$, 2, and 3 and $h(\xi)<h_0$ for all values of ξ.

As $h_0\to 1$, the limiting function $(G_0(h))^{-1/2}$ has an integrable singularity in (2.12), and hence, for large values of $|\xi|$, we have $h_0(\xi)\equiv 1$, i.e., the solution $h=h_0(\xi)$ corresponding to an infinitely thin interlayer $\zeta_0=0$ is a compacton. Solutions (2.12) can be used both to describe symmetric solitary waves and represent the front of intrusion flows at the interface between fluids. Figure 4 shows stationary solutions (2.12) for $\zeta_0=0$ and $\zeta_0=0.15$ and a photograph of the symmetric solitary wave realized in the experiment ($\mathrm{Fr}=0.488$ and $\zeta_0=0.15$). In this

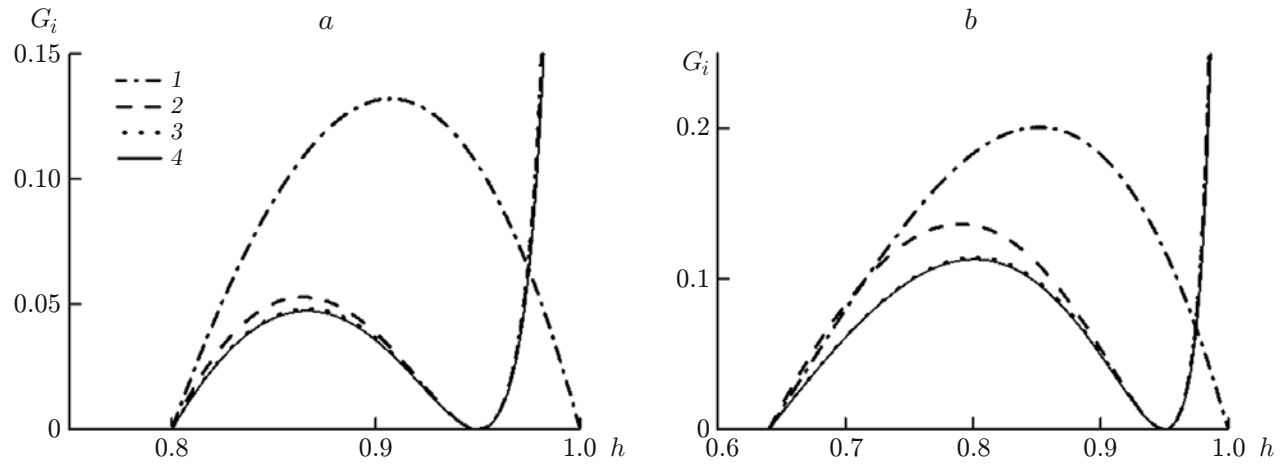

Fig. 3. Curves of $y = G_i(h)$ for $h_0 = 0.95$ and Fr = 0.40 (a) and 0.48 (b): $i = 0$ (1), 1 (2), 2 (3), and 3 (4).

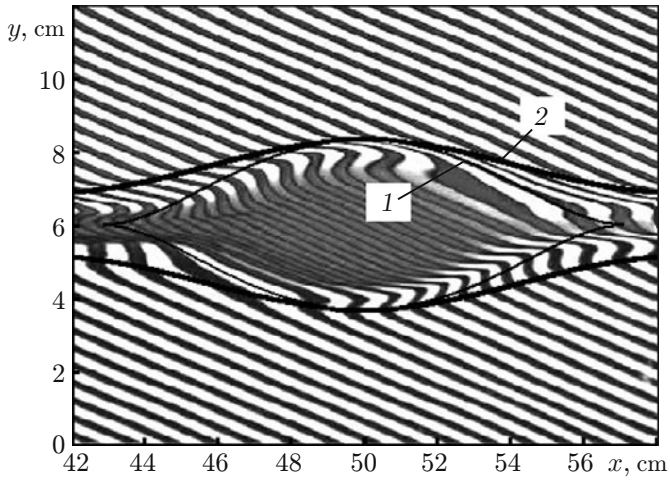

Fig. 4. Photograph of a solitary wave moving from left to right at the interface between the fluids (Fr = 0.488): 1) solution (2.12) for $i = 0$ and $\zeta_0 = 0$; 2) solution (2.12) for $i = 2$ and $\zeta_0 = 0.15$.

case, the solution with nonzero initial thickness of the interlayer (curve 2) specifies the outer boundary of the perturbations of the density field. We note that model (2.3) was obtained for $A/\zeta_0 \gg 1$ and, hence can be used to describe finite-amplitude waves only for a rather thin layer. At the same time, the wave considered has a moderate amplitude $A/\zeta_0 = 5.2$ relative to the thickness of the interlayer, and Eqs. (2.3) adequately describe the solitary-wave profile both for both thin interlayers and finite-thickness interlayers.

In the models used to construct traveling waves, dissipation effects were not considered. In real stratified fluids, solitary waves cannot propagate at constant velocity. Friction leads to a deceleration of solitary-wave propagation and corresponding change in the wave profile. Nevertheless, in a coordinate system attached to a solitary wave, the flow is quasistationary: at each time, the shape of the solitary wave coincides with the shape of a stationary wave of the same amplitude, allowing a comparison of the exact solution with experimental data. Because of the symmetry of the flows considered, the friction on the channel axis ($y = 1$) is equal to zero and the main contribution to energy dissipation comes from the processes at the interface between the intrusion and the surrounding fluid ($y = h(t, x)$) due to instability and turbulent mixing in the region of high velocity and density gradients. In the two-layer model, these effects can be taken into account only by supplementing relations (2.3) with terms due to turbulent friction at the interface between homogeneous layers. We also note that energy dissipation in a solitary wave is caused not only by friction on its boundaries but also by mass loss of the intrusion during its propagation because the total mass of the intermediate-density fluid transferred by the wave reduces with decreasing wave am-

plitude. Immediately behind the wave, the thickness of the interlayer increases compared to the unperturbed state, and differences between the exact solution and experimental data are observed only in a small region adjacent to the region of constant flow behind the wave (see Fig. 4).

Next, model (2.3) modified in view of friction is used to perform a numerical analysis of the nonstationary problem of the evolution of symmetric solitary waves in a two-layer fluid.

3. Solitary-Wave Decay. A comparison of models (2.2) and (2.3) for the stationary solutions representing traveling waves of various amplitudes shows that, for the investigated intrusion flows, these models provide close wave profiles over a wide range of determining parameters. Therefore, to analyze nonstationary flows, we confine ourselves to system (2.3), which is similar in structure to the Green–Naghdi equations for a one-layer fluid. In particular, for numerical implementation of this model, it is possible to use a generalization of the computation method for nonstationary flows proposed in [19]. In view of the dissipative effects caused by turbulent friction on the inner and outer boundaries of two-layer flow, for $h+\zeta=1$ and $Q=hu+\zeta w=0$ system (2.3) becomes

$$h_t+(hu)_x=0, \qquad w_t+(w^2/2+p)_x=(f_i-f^+)/\zeta,$$

$$\Big(hu^2+\zeta w^2+\frac{1}{2}\,h^2+\frac{1}{3}\,h^2\,\frac{d^2h}{dt^2}+p\Big)_x=-f^+-f^-, \tag{3.1}$$

$$f_i=c_i(u-w)|u-w|, \qquad f^+=c_w^+w|w|, \qquad f^-=c_w^-u|u|,$$

$$c_i\equiv\text{const}, \qquad c_w^\pm\equiv\text{const},$$

where f_i and $f^\pm$ are the shear stresses at the interface between the fluids and on the outer boundaries of the investigated flow region, respectively. As noted above, the specific features of the symmetric intrusion flow is that, on the channel symmetry axis $y=1$, the shear stress vanishes and $f^+=0$. This term is of significance only in experiments with a horizontal plate placed at the center of the channel (see Sec. 1). We also note that in the calculations presented below, accounting for friction at the channel bottom does not influence the flow pattern and we can set $f^-=0$. The values of the coefficients c_i and c_w^+ are chosen empirically and characterize the rate of mixing processes on the inner interfaces and in the vicinity of the plate.

A differential consequence of (3.1) are the inhomogeneous conservation laws

$$\Big(w^2+h^2+\frac{1}{3}\,h\Big(\frac{dh}{dt}\Big)^2\Big)_t+\Big(hu\Big(u^2+\frac{1}{3}\Big(\frac{dh}{dt}\Big)^2\Big)+\zeta w^3+2h^2u+\frac{2}{3}\,h^2u\,\frac{d^2h}{dt^2}\Big)_x$$

$$=-c_i|u-w|^3-c_w^+|w|^3-c_w^-|u|^3; \tag{3.2}$$

$$(Kh-hw)_t+\Big(Khu+\Big(\frac{1}{2}-h\Big)w^2+\frac{1}{2}\,h^2-\frac{2}{3}\,h\Big(\frac{dh}{dt}\Big)^2\Big)_x=-\frac{c_i(u-w)|u-w|}{\zeta}-c_w^-u|u|+\frac{c_w^+hw|w|}{\zeta}, \tag{3.3}$$

$$K=u+\frac{1}{3h}\Big(h^2\,\frac{dh}{dt}\Big)_x=u-\frac{1}{3h}\,(h^3u_x)_x.$$

In the absence of dissipation ($c_i=0$ and $c_w^\pm=0$), the additional law of energy conservation (3.2) can be used to construct solitary waves (see Sec. 2). The equation

$$h_t+(hu)_x=0 \tag{3.4}$$

and Eq. (3.3) form a closed system of conservation laws which is equivalent to the basic system (3.1). For numerical solution of the nonstationary problem of solitary-wave decay within the framework of model (3.3), (3.4), it is convenient to treat the functions h and $\Phi=h(K-w)$ as dependent variables. In these variables, the system takes a form similar to that of the Green–Naghdi equations for a one-layer fluid (see Eq. (10) in [19]). Therefore, below, we give only the main steps of the construction of the difference scheme.

The difference scheme used for the numerical solution of the initial-boundary-value problem for Eqs. (3.3) and (3.4) is formally a version of the Godunov scheme, in which the fluxes through the lateral boundaries of the meshes are calculated using the linearized Riemann problem. In turn, the Riemann problem is constructed using the characteristics of the equilibrium system without dispersion terms. For relations (3.3) and (3.4), the equilibrium system is the equations of two-layer shallow water [20, Chapter 4]

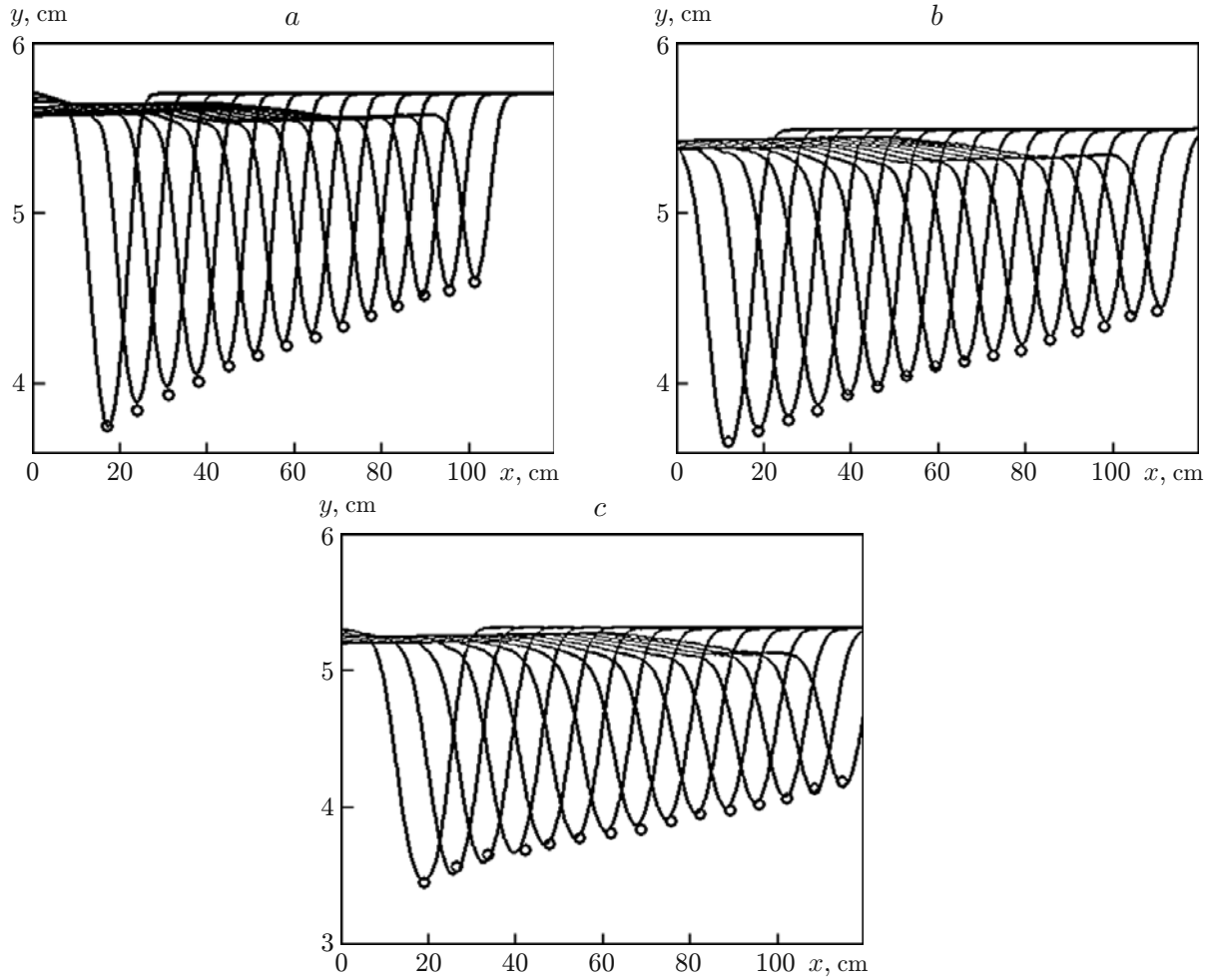

Fig. 5. Solitary-wave amplitude versus distance to the partition for various initial thicknesses of the interlayer (time interval between the points $\Delta t = 4$ sec): $\delta = 0.4$ (a), 0.6 (b), and 0.8 cm (c); the curves are the wave profiles simulated numerically, and the points are the corresponding positions of the wave crests obtained experimentally.

$$h_t + (hu)_x = 0,$$

$$(u - w)_t + (u^2/2 - w^2/2 + h)_x = 0, \tag{3.5}$$

$$hu + (1 - h)w = 0.$$

The equations for the characteristics (3.5) have the form

$$\frac{dx}{dt} = (1 - 2h)(u - w) \pm \sqrt{h(1 - h)(1 - (u - w)^2)}\,. \tag{3.6}$$

From (3.6) it follows that, for $|u - w| < 1$, system (3.5) is a hyperbolic system. We note that the basic system (3.3), (3.4) is not hyperbolic. The infinite velocity of perturbation propagation for system (3.3), (3.4) is implemented in finding the velocity u from the known variables h nd Φ by the linear equation

$$\frac{1}{3}\,h^3 u_{xx} + h^2 h_x u_x - \frac{hu}{1 - h} + \Phi = 0,$$

whose difference solution is found using the Thomas algorithm. The natural boundary conditions for system (3.3), (3.4) are the no-flux condition ($u = 0$) on the lateral boundaries of the flow region considered. The exact solution describing a solitary wave for model (2.3) is chosen as the initial conditions. Figure 5 gives sequential positions

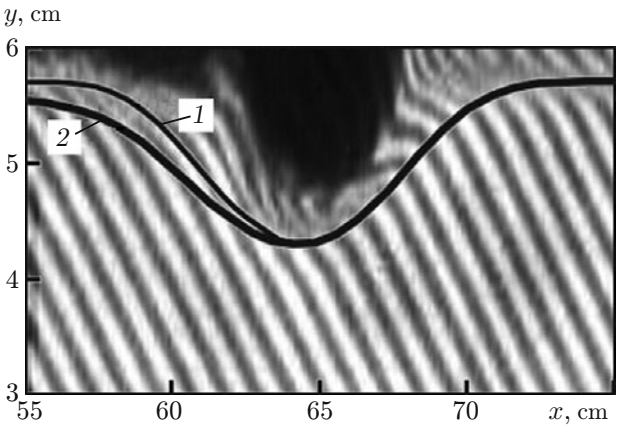

Fig. 6. Photograph of one of the implementations of the solitary internal wave shown in Fig. 5a: 1) solution (2.12) for $i = 2$; 2) numerical solution of the nonstationary problem.

of waves in dimensional variables calculated at regular time intervals $\Delta t = 4$ sec ($H = 6$ cm and $b = 2$ cm/sec^2). The points show the experimental positions of the wave crests for the same times. Figures 5a, 5b, and 5c differ in the initial thickness of the interlayer δ. For all calculations, the identical friction coefficients were used ($c_i = 0.012$ and $c_w^{\pm} = 0$). The calculation results show that the velocities of propagation and decay of solitary waves at the interface are adequately represented by dissipative terms of system (3.3), (3.4). Moreover, the effect of friction at the interface between the layers of different densities leads to asymmetry of the solitary-wave profile about the vertical axis through the crest. The thickness of the interlayer behind the numerically constructed wave increases, and the wave amplitude and mass of the transferred fluid decrease. Behind the wave, an expanding plateau occurs, which is followed by a nonstationary depression wave. Figure 6 gives the exact solution of (2.12) for $i = 2$ for the dissipationless model (curve 1) and the numerical solution (3.3), (3.4) (curve 2) which represents one of the realizations of the solitary wave shown in Fig. 5a. Figure 6 also shows a photograph of an internal solitary wave obtained experimentally. As in Fig. 4, the outer boundary of the wave is the boundary of deformation of the inclined lines caused by a perturbation of the density field due to the passage of the wave. A comparison of the stationary and nonstationary solutions (curves 1 and 2 in Fig. 6) shows that, at the leading edge of the wave, these solutions almost coincide and energy dissipation has a significant effect on the flow only behind its crest. We note that the constructed numerical solution also provides an important flow characteristic such as the rate of mass transfer from the wave. Therefore, the model considered is suitable for describing channel and pipe flows.

The stationary and nonstationary solutions of the solitary-wave problem constructed above also provide a formal description of the evolution of gravity flows in a horizontal channel under the effect of an initial momentum. However, experimental studies of interaction between a solitary wave and a plate placed horizontally in the plane of symmetry of the channel (see Sec. 1) show that there is a significant difference between the intrusion and the gravity flow in the vicinity of the plate (see Fig. 2), which is due to the activation of the mixing process resulting from the development of a boundary layer above the plate and under it. Hence, the transformation of the wave near the plate depends significantly on the initial thickness of the interlayer (compare Fig. 2a, c, and e and Fig. 2b, d, and f), and within the framework of a two-layer flow scheme, the assumption of the constant friction coefficient c_w^+ is inapplicable to the flow under the plate. Therefore, to interpret the experimental results for the evolution of the soliton behind the plate, we chose the friction coefficient in the vicinity of the plate according to the initial thickness of the interlayer so as to provide the corresponding energy dissipation of the gravity flow and, thus, to implicitly take into account the turbulent mixing effect.

Figure 7 shows the evolution of the profile of a solitary wave during its interaction with the plate calculated for model (3.3), (3.4) at equal time intervals $\Delta t = 2$ sec ($H = 8$ cm, $b = 2$ cm/sec^2, and $c_i = 0.012$). In addition, Fig. 7 shows the positions of the wave crests found experimentally for the same times during motion along the interface between the fluids (points 1) and in the gravity flow in the vicinity of the plate $l_1 < x < l_1 + l_2$ (points 2). From Fig. 7, it follows that the model adequately describes the amplitude and phase characteristics of the solitary

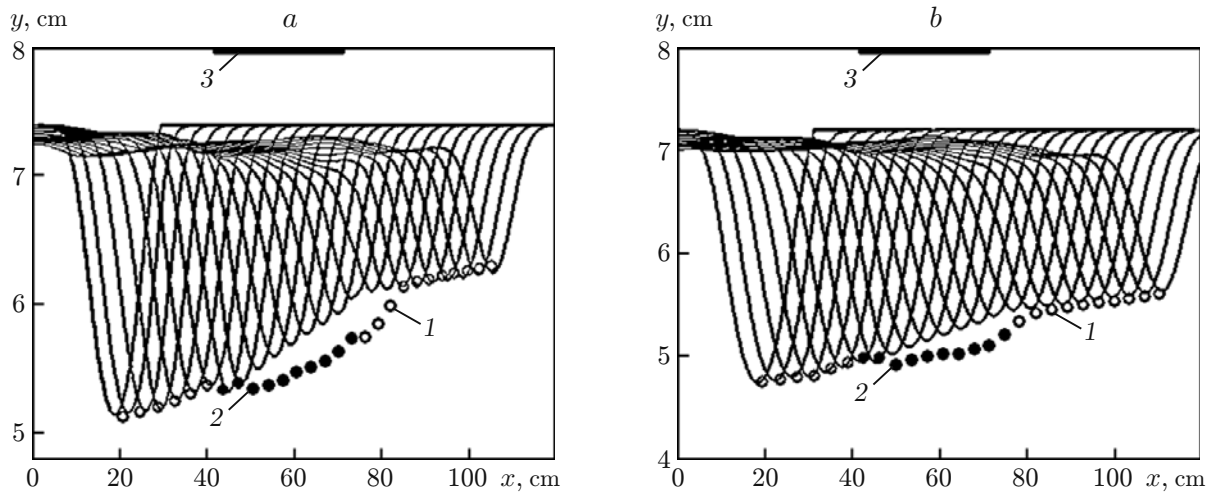

Fig. 7. Amplitude of the solitary wave incident on the plate versus distance to the partition at various initial interlayer thicknesses and friction coefficient (time interval between the points $\Delta t = 2$ sec): (a) $\delta = 0.6$ cm and $c_w^+ = 0.1$; (b) $\delta = 0.8$ cm and $c_w^+ = 0.05$; the curves correspond to the numerical calculation, and the points to the experimental positions of the solitary-wave crests at the interface (1) and under the plate (2); the plate is marked as 3.

wave ahead of and behind the plate; however, for a correct representation of the gravity flow in the vicinity of the plate, it is necessary to take into account turbulent mixing, which is beyond the scope of this model.

Conclusions. Symmetric internal solitary waves propagating along the interface between fluids of different densities are of interest for both physical and mathematical modeling. Investigation of the main features of the evolution of these waves under the action of an initial momentum allows one to understand some mechanisms of mass and momentum transfer in real flows in the atmosphere and ocean. Mathematical models (2.2)–(2.4) show that the formation of large-amplitude solitary waves at the interface of a two-layer fluid in a channel of finite depth is due to dispersion effects into the fluid surrounding the intrusion. Therefore, for the models considered above, soliton-like solutions have a limit as the thickness of the interlayer tends to zero. Thus, models (2.2)–(2.4) can be used to construct internal waves of large amplitude if by the amplitude is meant the relation A/δ.

In contrast to the energy dissipation mechanism for surface solitary waves in a homogeneous fluid, the energy dissipation mechanism for the waves generated by instability of the shear flow in the vicinity of inner interfaces is a fairly effective one. Therefore, an adequate model for internal solitary waves should take into account friction on the boundaries of the intrusion flow. A comparison of experimental data with the results of nonstationary numerical calculations performed for model (3.1) with a constant turbulent-friction coefficient shows that this model correctly represents solitary-wave decay at the interface. At the same time, the gravity flow structure in the vicinity of the plate (see Fig. 2) depends significantly on the initial thickness of the layer, and its description requires a more elaborate model that takes into account turbulent mixing in the vicinity of the wave front.

This work was supported by the Ministry of Education and Science of the Russian Federation (Grant No. 2.1.1/3543), the Russian Foundation for Basic Research (Grant No. 09-01-00427), Integration project No. 65 of the Siberian Division of the Russian Academy of Sciences, and Program No. 14.14 of the Russian Academy of Sciences.

REFERENCES

1. A. Scotti and J. Pineda, "Observation of very large and steep internal waves of elevation near the Massachusetts coast," *Geophys. Res. Lett.*, **31**, L22307, 1–5 (2004).
2. K. R. Helfrich and W. K. Melville, "Long nonlinear internal waves," *Annu. Rev. Fluid Mech.*, **38**, 395–425 (2006).

3. C. L. Stevens, T. S. R. Fisher, and G. A. Lawrence, "Turbulent layering beneath the pycnocline in a strongly stratified pit lake," *Limnol. Oceanogr.*, **50**, No. 1, 197–206 (2005).
4. T. B. Benjamin, "Internal waves of permanent form in fluids of great depth current," *J. Fluid Mech.*, **29**, 559–592 (1967).
5. R. E. Davis and A. Acrivos, "Solitary internal waves in deep water," *J. Fluid Mech.*, **29**, 593–608 (1967).
6. T. Maxworthy, "On the formation of nonlinear internal waves from the gravity collapse of mixing regions in two and three dimensions," *J. Fluid Mech.*, **96**, 47–64 (1980).
7. T. W. Kao and K. H.-P. Pao, "Wave collapse in the thermocline and internal solitary waves," *J. Fluid Mech.*, **97**, 115–128 (1980).
8. K.-K. Tung, T. F. Chan, and T. Kubota, "Large amplitude internal waves of permanent form," *Studies Appl. Math.*, **66**, 1–44 (1982).
9. H. Hohji, N. Matsunaga, Y. Sugihara, and K. Sakai, "Experimental observation of internal symmetric solitary waves in a two-layer fluid," *Fluid Dyn. Res.*, **15**, 89–102 (1995).
10. A. P. Stamp and M. Jacka, "Deep-water internal solitary waves," *J. Fluid Mech.*, **305**, 347–371 (1995).
11. N. P. Schmidt and R. H. Spigel, "Second-mode internal waves I, II," in: *Proc. of the 5th Int. Symp. on Stratified Flows* (Vancouver, Canada, 10–13 July, 2000), Univ. of British Columbia, Vancouver (2000), pp. 809–820.
12. D. G. Akhmetov, *Vortex Rings*, Springer, Berlin–Heidelberg (2009).
13. N. V. Gavrilov and V. Yu. Liapidevskii, Symmetric solitary waves at the interface between fluids," *Dokl. Ross. Akad. Nauk*, **429**, No. 2, 187–190 (2009).
14. E. V. Ermanyuk and N. V. Gavrilov, "A note on the propagation speed of a weakly dissipative gravity current," *J. Fluid Mech.*, **574**, 393–403 (2007).
15. N. V. Gavrilov and E. V. Ermanyuk, "Diffraction of internal waves by a circular cylinder near the pycnocline," *J. Appl. Mech. Tech. Phys.*, **40**, No. 2, 258–262 (1999).
16. E. V. Ermanyuk and N. V. Gavrilov, "Interaction of an internal gravity current with a submerged circular cylinder," *J. Appl. Mech. Tech. Phys.*, **46**, No. 2, 216–223 (2005).
17. W. Choi and R. Camassa, "Fully nonlinear internal waves in a two-fluid system," *J. Fluid Mech.*, **396**, 1–36 (1999).
18. K. R. Helfrish, "Decay and return of internal waves with rotation," *Phys. Fluids.*, **19**, No. 2, 026601 (2007).
19. O. Le Métayer, S. Gavrilyuk, and S. Hank, "A numerical scheme for the Green–Naghdi model," *J. Comput. Phys.*, **229**, No. 6, 2034–2045 (2010).
20. V. Yu. Liapidevskii and V. M. Teshukov, *Mathematical Models of Long-Wave Propagation in an Inhomogeneous Fluid* [in Russian], Izd. Sib. Otd. Ross. Akad. Nauk, Novosibirsk (2000).